J Mater Sci (2021) 56:13814–13826

Metals & corrosion

Interaction of stress relaxation aging behavior and microstructural evolution in Inconel 718 alloy with different initial stress status

JiaJia Zhu[1], WuHua Yuan[1,*], Fei Peng[1], and Qiang Fu[1]

[1] School of Materials Science and Engineering, Hunan University, Changsha 410082, China

Received: 24 November 2020
Accepted: 4 May 2021
Published online: 18 May 2021

ABSTRACT

The two-stage aging treatment with different initial loading stresses were carried out in the Inconel 718 alloy after solution annealing process to investigate the stress relaxation and age hardening behaviors on basis of microstructural evolution. The result showed that the stress relaxation behavior mainly occurred in the first aging stage and the corresponding mechanism changed from diffusion creep with initial loading stress of 100 MPa into dislocation slip with initial stress of 600 MPa. Simultaneously, the influence of initial stress on yield strength was counteracted balanced the creep recovery and dislocation hardening, resulting in nearly constant value if yield strength. During the secondary aging stage, the strength of the purely aged sample is 3% higher than that of the high initial stress sample, and the precipitated phase morphology distribution is more uniform. The stress relaxation occurred in the secondary aging stage was negligible, irrespective of initial stress status. In condition, the application of initial stress gave rise to the precipitation behavior, which presented faster growth and coarsening with increasing initial stress value. As a comparison, the distribution of precipitates in sample without loading stress relatively more homogeneous and revealed denser, leading to higher yield strength compared with other samples with initial stress.

Introduction

Superalloy is a kind of metal material with good high temperature strength, and other fantastic comprehensive properties under above 600 °C [1]. As a representative superalloy, Inconel 718 alloy is an aging precipitation-hardening nickel-based superalloy. During the aging process of Inconel 718 alloy, there are mainly three precipitation phases of γ'' phase, γ' phase, and δ phase, which are precipitated from the γ matrix [2, 3]. The γ'' phase (Ni_3Nb, DO_{22})

Handling Editor: David Balloy.

Address correspondence to E-mail: yuan46302@163.com

https://doi.org/10.1007/s10853-021-06144-1

is the main strengthening phase of Inconel 718 alloy, which is generally disk-shaped [4]. The γ' phase is the secondary strengthening phase of Inconel 718 alloy, the main component is $(Ni_3(Al, Ti))$, which is generally spherical and has a face-centered cubic LI_2 structure [5, 6]. The δ phase is a stable coherent phase with an orthorhombic DO_a crystal system structure and the chemical formula is (Ni_3Nb) [7, 8].

Inconel 718 generally adopts a standard heat treatment process including a combination of solid solution strengthening and two-stage aging precipitation strengthening to ensure the required mechanical properties, microstructure and dimensional accuracy of the parts [9, 10]. During solution heat treatment, in order to ensure that the supersaturated solid solution is fixed and not be decomposed, a faster quenching speed is generally adopted. However, a great amount of quenching residual stress will be introduced. During the subsequent aging heat treatment stage, the strengthening phase will gradually precipitate inside the grain to obtain the desired precipitation hardening and mechanical properties. In addition to microstructure evolution, thermally activated creep and stress relaxation also occur simultaneously during aging process [11, 12]. Fruitful works have been reported on the relaxation of residual stress via aging treatment. Rahimi [13] established a numerical model to describe the stress relaxation behavior of Inconel 718 alloy during aging heat treatment. Aba-Perea [12] found that the combination of plastic relaxation and early creep relaxation of Inconel 718 alloy resulted in 60% relaxation of quenching stress in the heating stage of aging. Actually, it has been reported that the variation of stress field inside superalloy play a crucial role on the precipitated behavior of strengthened phases. Qin [15] found that the external stress strongly promote the nucleation and precipitation of the γ'' phase in the early stages of aging. As a whole, the related articles of superalloys mainly focus on the establishment of aging-stress relaxation model [13, 14], precipitated kinetics of strengthening phase [15–17] and characteristics of residual stress [12]. However, the research on the relationship between stress relaxation and age hardening behavior is limited.

This paper studies the stress relaxation aging behavior and strength evolution in Inconel 718 alloy during the two-stage aging process. Different loading stresses are applied to the alloys to determine the effect of initial stress on the high temperature relaxation characteristics during the aging process. The purpose of this study is to reveal the interaction between age hardening and stress relaxation behavior, and to provide guidance for the control of residual stress and the strengthening of precipitates in superalloys.

Experimental program

Materials and experimental procedures

The material chosen for this study is industrial Inconel 718 superalloy, whose main chemical composition, supplied by the manufacturer, is provided in Table 1. The as-received materials were machined into a ∅20 × 300 mm rod-shaped sample to solution heat treatment at 970 °C for 1 h, and then water quenched. The as-quenched sample was made into a stress relaxation sample with ASTM standard [18] dimension shown in Fig. 1. Subsequently, the stress relaxation test at two-stage aging treatment was applied and the corresponding parameter are shown in Fig. 2. Finally, the samples after aging treatment were air-cooled to room temperature, followed by tensile experiment. In order to determine the aging hardening effect and strength evolution caused by the precipitated in the stress-relaxation-aging stage, the interrupted stress relaxation test was conduct followed by tensile test at ambient temperature. The interrupted stress relaxation test was carried out on an Instron 8862 machine with constant strain level within a specified aging time followed by unloaded and cooled in air to room temperature. Finally, the aging samples were subjected to tensile test on an Instron 3369 machine at room temperature.

Stress-relaxation aging treatment

During the stress relaxation experiment, the temperature is strictly controlled within ± 1 °C through three thermocouples connected at the gauge length of the sample, and an extensometer was installed to control the strain of the sample. The test procedure is shown in Fig. 2. In the first stage of stress relaxation aging, the sample was firstly held for 10 min and then loaded to the specified stress level at a rate of the 2.83 MPa/s (i.e., 100–300–600 MPa), during which constant strain was used to study the stress relaxation behavior. After the first stage of heat treatment, the

Table 1 Main chemical composition of Inconel 718 alloy

Elements	Ni	Cr	Fe	Mo	Nb	Al	C	Ti
(wt %)	Balanced	18.90	18.60	3.06	5.10	0.45	0.04	0.90

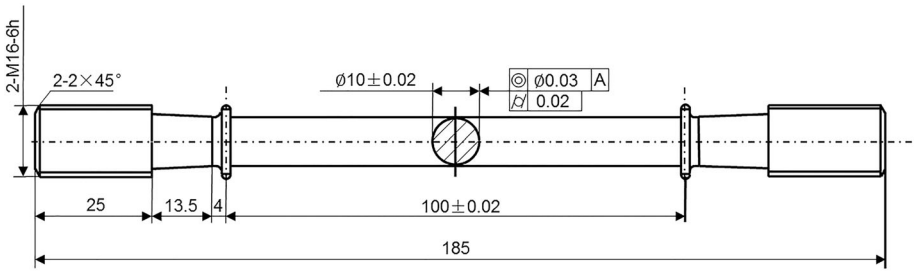

Figure 1 Dimensional drawing of the stress relaxation tensile specimen (Unit: mm).

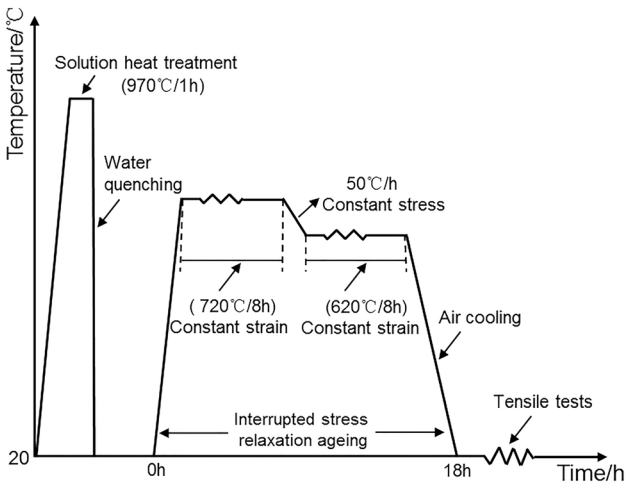

Figure 2 Schematic diagram of sample preparation and testing procedure.

furnace temperature was reduced to 620 °C at a rate of 50 °C/h. During the cooling process, the sample were controlled by constant stress. When the furnace temperature reached 620 °C, the control mode of the sample was changed to constant strain control again until the end of the test. The control method of the intermittent stress relaxation test was also strictly in accordance with the above process.

Microstructural characterization

Electron backscatter diffraction (EBSD) observation was performed on samples under different initial loading stresses. The samples were prepared with 10 vol% $HClO_4$ and 90 vol% CH_3OH solution under the voltage of 15 V for 15–20 s. The distribution of grain boundary disorientation was examined on a FEI Quanta-200 field emission gun scanning electron microscope (SEM) equipped with an EBSD detector. In this study, a step size of 1.4 μm was utilized, and the collected data was analyzed by OIM software. Furthermore, TEM observation was carried out on some representative samples after stress relaxation aging test. For TEM observation, the sample were mechanically polished to 60 μm, followed by twin-ject electropolishing with chemical solution (i.e., 5 vol% $HClO_4$ and 95 vol% CH_3OH) at −30 °C and checked on a JEM-3010 transmission electron microscope.

Result

Stress relaxation behavior during the aging stage

Stress relaxation curves with different initial stresses

Figure 3 shows the stress relaxation curves of superalloy samples with different initial stresses. Based on the variation of temperature, the stress change in the entire two-stage aging process can be divided into three stages, indicated as first aging stage, cooling stage and secondary aging stage, respectively (Fig. 3a). During the first stage, the stress was relaxed rapidly and is closely related to the value of initial stress. It is worthwhile mentioning that the stress relaxation curve at the onset of the first aging stage, which was significantly different from that of traditional reported result with an obvious threshold stress [13]. Then there is a constant stress control stage where the temperature cooling from 720 to 620 °C, during which the stress remains constant. Finally, there was the steady-state stress process in secondary aging stage. The stress in this stage did not relax and shows a stable and slightly increasing trend.

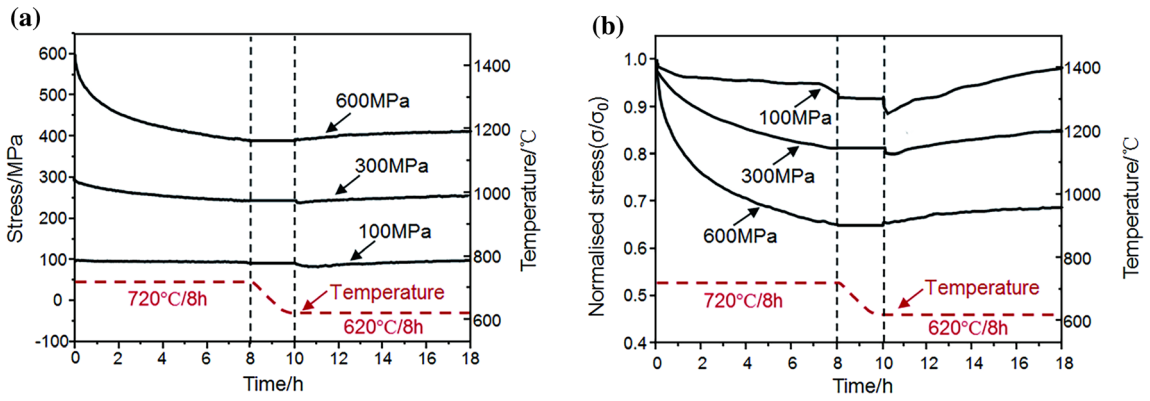

Figure 3 **a** Stress relaxation curves, **b** the curves shown in **a** normalized by the initial stresses during two-stage aging condition; the temperature is indicated by the dashed line and σ_0 is the initial loading stress.

In addition, the stress relaxation results are normalized as shown in Fig. 3b. Obviously, the stress relaxation behavior depends on the value of initial stress during the first stage, while the stress relaxation behavior in the secondary aging stage is hardly affected by it. When the initial stress was 100 MPa, marginal relaxation was observed in the sample. Moreover, the stress reduction monotonically increased up to 8.3% in the first aging stage, while inversely decreased the secondary aging. As result, the stress was only relaxed by 1.3% after two-stage aging treatment. At low stress levels, the sample hardly undergoes stress relaxation. With the initial stress loading to 300 MPa, the stress reduction increased to 18.7% during the first aging stage, and the stress reduction was 15.4% after the steady-state relaxation during the secondary aging stage. When the initial stress was loaded to the vicinity of yield strength (i.e., 600 MPa), the sample undergoes significant stress relaxation in the first-stage aging stage, and corresponding the stress reduction was 35%. Finally, as the stress during the secondary aging stage increased slightly, the stress reduction after two-stage aging was 31.4%.

Stress relaxation mechanism with different initial stresses

As we all know, stress and temperature can change or control the creep mechanism. Broadly speaking, stress relaxation is a special form of creep [19]. The essence of stress relaxation is the gradual transformation of elastic strain into permanent plastic strain, while the total strain remains constant, thus satisfying the following equation [20, 21]:

$$\varepsilon_{\text{tol}} = \varepsilon_e + \varepsilon_p + \varepsilon_c \tag{1}$$

$$\frac{d\varepsilon_t}{dt} = \frac{d\varepsilon_e}{dt} + \frac{d\varepsilon_c}{dt} \tag{2}$$

Since the total strain is constant, according to Hooke's law, $\varepsilon_e = \sigma/E$ then:

$$\frac{d\varepsilon_c}{dt} = -\frac{d\varepsilon_e}{dt} = -\frac{d\sigma}{Edt} = \dot{\varepsilon} \tag{3}$$

where ε_{tol} is the total strain, ε_e is the elastic strain, ε_p is the plastic strain caused by the initial loading stress, S is the creep strain, and E is the elastic modulus of the material. The stress relaxation is a thermal activation process, which conforms to the Arrhenius and Norton equations. The relationship between strain rate, stress and temperature can be expressed as:

$$\dot{\varepsilon} = A\sigma^n \exp\left(-\frac{Q}{RT}\right) \tag{4}$$

where A is a dimensionless constant for a given materials,σ is the applied stress, Q is the deformation activation energy, R is the gas constant, generally 8.314 J mol^{-1} K^{-1}, T is the absolute temperature, and n is the stress exponent, which can be obtained by the logarithmic strain rate and the slope of the logarithmic stress. Then there are:

$$\ln\dot{\varepsilon} = \ln A \exp\left(-\frac{Q}{RT}\right) + n\ln\sigma \tag{5}$$

According to the relationship between the steady-state creep strain rate and the stress value in the equation, the value of n for a specific material can be obtained. The expression is:

$$n = \frac{\partial \ln \dot{\varepsilon}}{\partial \ln \sigma} \tag{6}$$

The stress relaxation mechanism at high temperature usually includes atomic diffusion, dislocation slip and climbing and so on. Stress exponent n is frequently used to analyze the stress relaxation mechanism [22]. $n = 1$ indicates diffusional creep [23, 24]; When $n = 2$–3, diffusion and dislocation climbing occur simultaneously [25, 26]; When n ranges from 4 to 9, the relaxation process is dominated by dislocation slip mechanism [27, 28]. Figure 4 shows the value of the power-law stress exponent n during the first-stage aging process calculated according to Eqs. (4) and (6). When the initial loading stress is 100 MPa, 300 MPa, 600 MPa, the calculated stress exponent n values are 1.26, 7.35 and 8.07, respectively. These n values indicate that under low stress loading conditions, the stress relaxation mechanism is dominated by diffusion creep. When the initial stress increases, the stress relaxation mechanism gradually shifts to a dislocation slip mechanism. The dislocation caused by the change of the initial loading stress can significantly change the stress relaxation mechanism of Inconel 718 alloy.

Aging hardening behavior with different initial stresses

For precipitation-strengthened Inconel 718 alloy, aging heat treatment is one of the main means to improve its strength. During the aging process, not only the relaxation of the stress field, but also the aging strengthening of the precipitated phases will arise. Figure 5 shows the changes in yield strength with time under different initial loading stresses. At the beginning of the first aging stage, the yield strength increased rapidly, whilst the strength of aged samples under loading condition was significantly lower than that of pure aged samples. In the remaining part of the first aging stage, the strength gradually increases with prolonging the aging time, while the influence of initial loading stress on yield strength drastically weakened. Finally, the yield strength of the two samples after first aging present nearly the same. During the secondary aging processing, the strength increased slowly with time. Compared with the strength of the purely aged samples, the presence of the initial loading stress inhibits the strength of the material. After the final two-stage aging, the pure aging sample has a higher yield strength. Table 2 shows the specific yield strength and stress relaxation values at different aging stages.

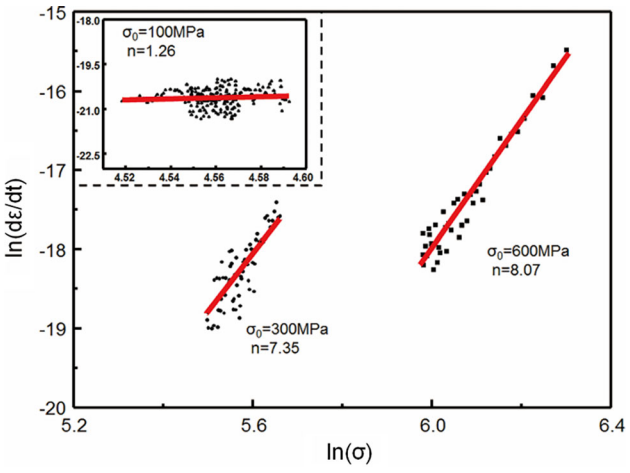

Figure 4 The creep stress exponent n value with different initial loading stresses in the first aging stage. The upper left corner is the schematic diagram of the ln (σ)-ln ($d\varepsilon/dt$) relationship in sample when the initial stress is 100 MPa.

Microstructure characterization

In order to depict the microstructure characteristics of sample after aging treatment, the sub-structure and crystallographic variation were detected by EBSD technique and the corresponding resulting are shown in Figs. 6 and 7. Due to the relatively low aging temperature, there's not enough grain growth or recrystallization, which means that the grain size was nearly the same at that of virgin state (20 ± 0.5 μm). Figure 6 shows that with the increase of initial

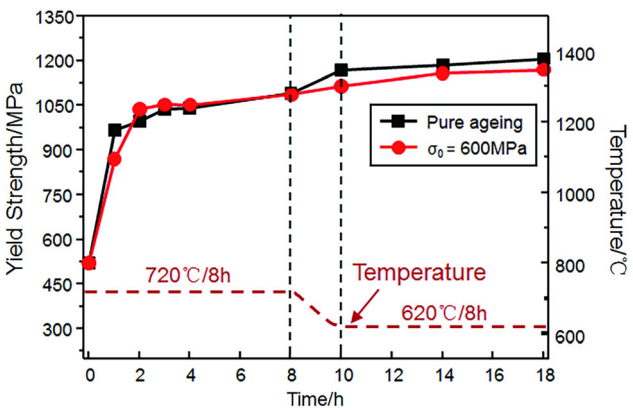

Figure 5 Change of yield strength during stress relaxation aging process.

Table 2 Yield strength and stress relaxation values during the aging stage under different initial loading stresses

Initial loading stresses	$\sigma_0 = 0$MPa Yield strength	Yield strength	$\sigma_0 = 600$MPa stress relaxation values
First aging stage	1090 MPa	1086 MPa	390 MPa
Secondary aging stage	1206 MPa	1169 MPa	412 MPa

loading stress, the volume fraction of low angle grain boundary (LAGB) increased from 4.8% to a saturated value of 11.8% in the case of 300 MPa, followed by a sudden reduction to 7.3% as loading stress increased to 600 MPa. Actually, the loading stress of 0–300 MPa is smaller than the yield strength (587 MPa), while the stress of 600 MPa has exceeded.

Furthermore, Fig. 7 was a schematic diagram of the misorientation angle distribution of the samples under different initial loading stresses after stress relaxation aging. The peak in the misorientation angle shown in Fig. 7 was at the $60° < 111 >$ misorientation, corresponding to the Σ3 misorientation relationship in the coincidence site lattice (CSL). The change of the relationship between the Σ3 twin boundary and the initial loading stress is consistent with the high angle change trend. With initial loading stress increased, the volume fraction of

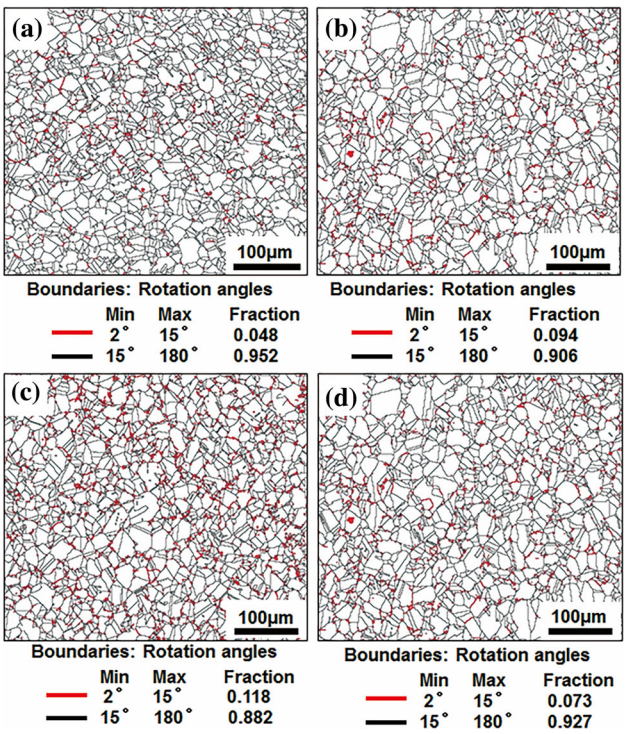

Figure 6 EBSD grain boundary orientation distribution of samples during two-stage aging with different initial loading stresses, **a** purely aged state, **b** 100 MPa, **c** 300 MPa, **d** 600 MPa.

Σ3 twin boundary decreased from 28.9 to 19.5% in the case of 100 MPa, and then increased to 25.3% at the initial stress of 600 MPa. When the initial loading stress below the yield strength, less effect on the Σ3 twin boundary. The variation of initial loading stress scarcely influenced the characteristics of Σ3 twin boundary, while the volume fraction increases with the initial loading stress near the yield strength.

Besides, the TEM morphology were exhibited in Figs. 8 and 9 to delve into the evolution of the precipitated phases during the first aging stage with different initial loading stresses. Figure 8a–d were the morphologies of the precipitates when the initial loading stress was 0 MPa (purely aged state), 100 MPa, 300 MPa, and 600 MPa, respectively. Figure 8e–h corresponds to the dark field image with initial loading stress of 0 MPa (purely aged state), 100 MPa, 300 MPa, and 600 MPa. It can be seen that the initial loading stress promotes the growth of the γ'' phase after the first aging stage. In contrast to the precipitates of purely aged sample in Fig. 8a, the γ'' phase in the sample with an initial loading stress of 600 MPa was larger in size, ranging from around 14–22 nm, while smaller in density. As to the sample with initial loading stress of 300 MPa, it was found that dislocation slip has occurred during the first aging stage (Fig. 9a), consistent with the result of Fig. 4. Furthermore, some dislocation was observed to be pinned by δ phase that located at grain boundary, as shown in Fig. 9b.

During the secondary aging stage, the TEM morphology of precipitated phases in Fig. 10 (a–c) and (d–f) presents purely aged sample, as well as the sample with initial loading stress of 600 MPa in Inconel 718 alloy. It can be found that the γ'' phase maintains a good coherent relationship with the matrix, and a small quantity of dislocations were observed inside the matrix, while a mass of dislocations were aggregated and entangled at the grain boundaries. Compared with the purely aged samples, the density and size of the γ'' phase with initial loading stresses showed distinct differences.

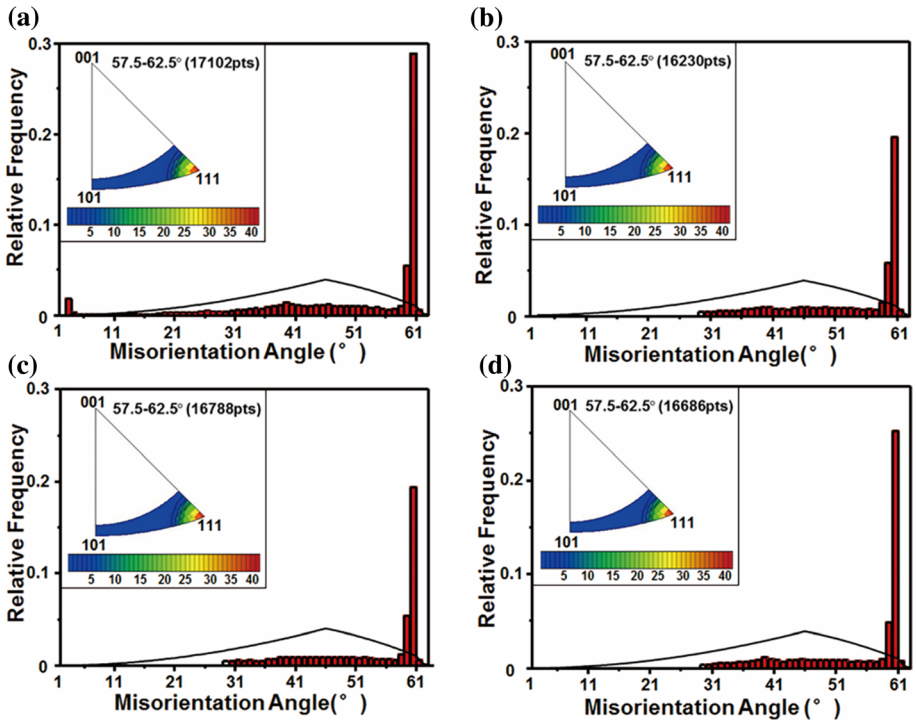

Figure 7 Distribution of misorientation angles of two-stage aging specimens under different initial loading stresses, **a** purely aged state, **b** 100 MPa, **c** 300 MPa, **d** 600 MPa. The inserted images inside each figure indicate the rotated axis distribution corresponding to the misorientation angle range 57.5–62.5.

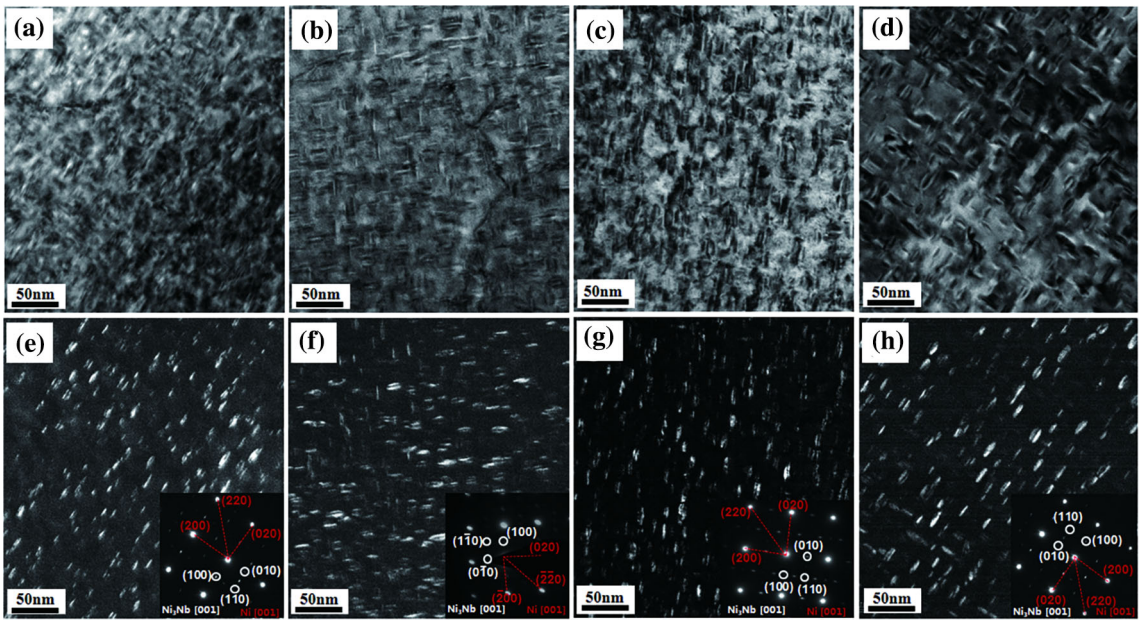

Figure 8 TEM schematic diagram of samples with different initial loading stresses after the first aging stage. **a** Purely aged sample, **b** Sample with initial loading stress of 100 MPa, **c** Sample with Initial loading stress of 600 MPa, **d** Dark field image of purely aged sample, **e** Dark field image of the sample with initial loading stress of 100 MPa, **f** Dark field image of the sample with initial loading stress of 600 MPa.

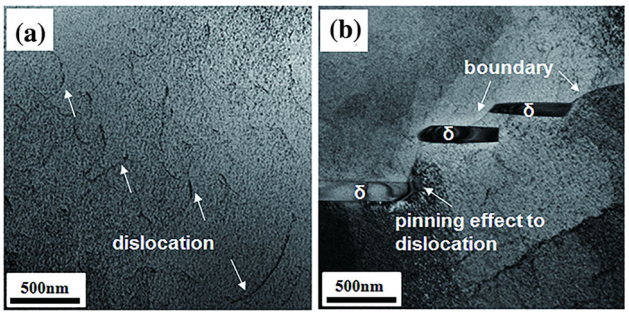

Figure 9 TEM schematic diagram of samples with initial stress of 300 MPa after the first aging stage. **a** Dislocation distribution, **b** Dislocation pile-up around δ phase.

Discussion

Stress relaxation mechanism during the aging process

The stress relaxation of alloys under conditions of aging temperature and loading stress is usually attributed to the creep deformation issued from the movement of dislocations [29, 30],and the change of microstructure is the main reason for the variation of stress relaxation mechanisms in Inconel 718 alloy with different initial stresses. As to the samples with identical heat treatment and different initial loading stresses, the variation of stress as a function of time showed a typical three-stage stress relaxation behavior (Fig. 3), that is, the rapid stress relaxation at the first aging stage, the constant stress at the cooling stage and the steady-state stress at the second aging stage.

During the first aging process, the degree of stress relaxation with low initial stress and high initial stress was significantly different, which means that the potential stress relaxation mechanism of Inconel 718 alloy changed with the increase of initial stress. When the initial stress applied to the materials was 100 MPa, which was much smaller than the yield strength and hence existed as the long-range stress field among the material. Accordingly, the dislocation density was small and dislocation cannot slip [31]. In this situation, the diffusion velocity of atoms increased and the stress relaxation mechanism was diffusion creep.

With the initial stress increased to 300 MPa, a certain elastic strain will be generated during the initial stage of aging process, and the corresponding

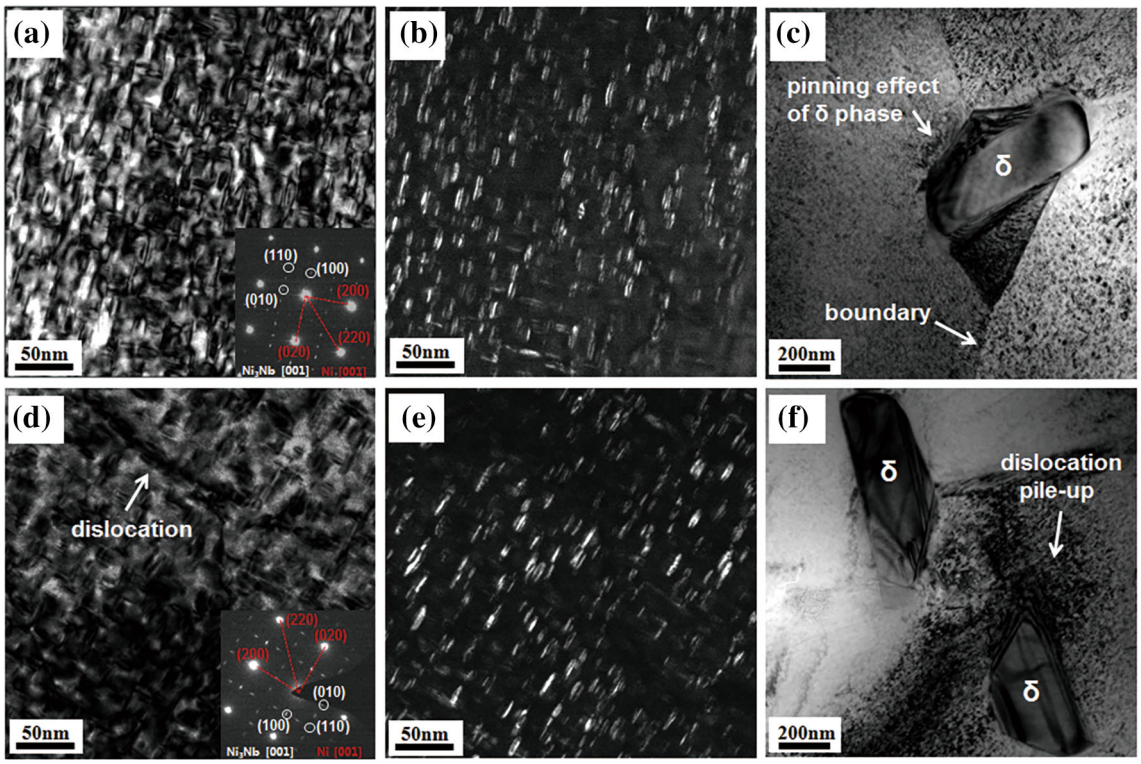

Figure 10 TEM schematic diagram of samples with initial stresses of **a**–**c** 0 MPa and **d**–**f** 600 MPa after two-stage aging. Where **a d** precipitation phase morphology, **b e** dark field image, **c f** pinning effect of δ phase to dislocation movement.

internal elastic stress was relatively large. Subsequently, the elastic strain generated inside the material gradually changes into plastic strain through the deformation mechanism such as atomic diffusion or dislocation motion [32], and the dominant mechanism of stress relaxation changes from diffusion creep into dislocation slip.

When the initial loading stress approaches the yield strength (i.e., σ_0 = 600 MPa), dislocation slips across obstacles by the combined effect of external stress and thermal activation [33], and the stress relaxation mechanism is dominated by dislocation slip. In this case, the dislocation propagated during plastic deformation, leading to the intersection and tangle of dislocation via different slip systems, as well as the formation of dislocation cell [34]. Meanwhile, dynamic recovery occurred and resulted in the dislocation annihilation and rearrangement [35]. Under the coupled influence of plastic deformation and dynamic recovery, the dislocations distributed in the vicinity of cell wall gradually arranged neatly to form a substructure, and the cell structure finally turned into a subgrain (Fig. 6).

During the cooling stage, the stress remains constant by stress control. Then in the secondary aging stage, the stress relaxation curve shows a similar trend of slight increase in stress, and the stress relaxation behavior was not affected by the initial loading stress (Fig. 3). During this process, the driving force of dislocation creep was insufficient due to the decrease of temperature compared with the first aging stage. Studies [36, 37] have shown that only a small amount of atomic diffusion and slight plastic deformation occurs at relatively low temperatures, but the increase of available vacancies and paths at grain boundaries promotes diffusion creep. Due to the simultaneous occurrence of age hardening, the stress relaxation resistance at this stage increases significantly. Because of the increase in stress relaxation resistance and the decrease in temperature, the stress relaxation behavior of the alloy during the secondary aging stage was hardly affected by the initial loading stress. In addition, the stress fluctuations during the secondary aging stage was also observed and can be ascribed to that the temperature decrease makes the thermal activation more difficult to occur and the external stress required for dislocations movement increases, leading to the increase of flow stress [38].

Precipitation behavior and aging hardening during stress relaxation process

As is well known, the essence of stress relaxation is considered as a process that elastic deformation gradually transforms into plastic deformation [39]. In the case of constant temperature, the increase in initial stress was not only favorable to the generation of plastic deformation, but also promoted the formation of precipitates. For Inconel 718 precipitation strengthening alloy, the increase in precipitation strengthening effect is mainly related to the characteristics of γ'' phase, such as volume fraction and size as well as the anti-phase boundary energy [40, 41]. As a result, the stress relaxation process was coupled with the precipitation of γ'' phase and aging hardening, which concurrently influenced the variation of mechanical properties during aging process.

Analysis of microstructural evolution and mechanical properties during the first aging stage

The precipitation behavior of strengthening phase in Inconel 718 alloy significantly depended on the heat treatment. During the rapid cooling process after solution treatment, the time is insufficient for the precipitation of strengthening phase γ'' and γ' inside γ matrix, resulting in the relatively lower strength. As the heat treatment processed into the first stage, the strengthening phase γ'' was precipitated adequately due to the existence of abundant nucleation sites. With prolong of aging time, the amount of γ'' phase increased, which was the main reason of improved yield strength via the pinned effect.

Moreover, the stress relaxed rapidly at the onset of the first aging stage, while still revealed a relatively discrepancy at different initial loading stress levels, as shown in Figs. 3a and 5. As higher stress can facilitate the formation of precipitates during the creep aging process, the nucleation rate of the precipitated phase increases rapidly. However, due to its short time, the γ'' phase has no time to grow up, and the yield strength presented slightly lower than that of the pure aging state. In this process, the supersaturation of the γ'' phase is close to the equilibrium value [16].

In the remaining part of the first aging stage, the volume fraction of γ'' phase of the purely aged and stress relaxation state samples gradually stabilized. With prolong aging time, number of γ'' phase nucleation sites in purely aged sample increased, whilst the

existence of the initial loading stress increases the size of the γ'' phase as shown in Fig. 8. Eventually, the strengthening effect of abundant precipitates in stress relaxation sample was counteracted by the coarsening process and the yield strength of the two samples presents nearly the same. Correspondingly, a schematic diagram of the interaction between precipitates and dislocations with different initial loading stresses during the stress relaxation aging process is proposed in Fig. 11.

Comprehensive analysis of microstructural characteristics and mechanical performance during the secondary aging stage

Although the applied initial stress hardly influenced the yield strength of the first aging stage, it will obviously affect the characteristics (number and size of nucleation) of the precipitated phases, and further affect the corresponding strengthening behavior during the secondary aging stage. In comparison with first aging stage, the secondary aging stage dominantly controlled the growth rate of γ'' phase, which slowed down due to the decrease of aging temperature. This influence not only ensures the precipitation of the strengthening phase, but also prevents the coarsening of precipitated phase. As a result, the γ' phase precipitated as fine particles at this stage to produce a strengthening effect.

In terms of the variation of mechanical performance (see Fig. 5), the application of initial loading stress slightly influenced the aging strengthening behavior. As shown in Table 2, the yield strength of the specimen after two-stage aging with an initial loading stress of 600 MPa was 3% lower than that of the specimen with 0 MPa. Moreover, it is also found that the characteristics of γ'' phase changed with initial stress in sample after the first aging stage (Figs. 8 and 9). It should be noted that the γ'' phase still maintains the discrepancies in quantity and density after secondary aging stage (see Fig. 10). Consequently, higher initial stress will introduce larger creep, which will lead to faster growth and coarsening of precipitates after two-stage aging treatment, and intensified dislocation movement (see Fig. 10f), which is manifested as a difference in strength.

Overall, there is ting change in the low-angle and high-angle grain boundary content at a low initial loading stress of 100 MPa (see Fig. 6a, b) compared with that of the purely aged samples, indicating that recovery creep hardly occurs. Hence, the dislocations caused by creep strain are basically negligible, and the existence of initial stress will generate a larger lattice space and facilitate the diffusion of atoms, which manifests that the stress relaxation mechanism was mainly diffusion creep.

As the initial loading stress increased to 300 MPa, the low-angle grain boundary fraction increased from 4.8 to 11.8% (see Fig. 6a, c), indicating that recovery and primary strain hardening have reached a balance to some extent. However, a small amount of dislocations are activated, which leads to an increase in the number of sub-structure (see Fig. 6a, c). In other words, the stress relaxation mechanism was transformed into dislocation slipping and climbing.

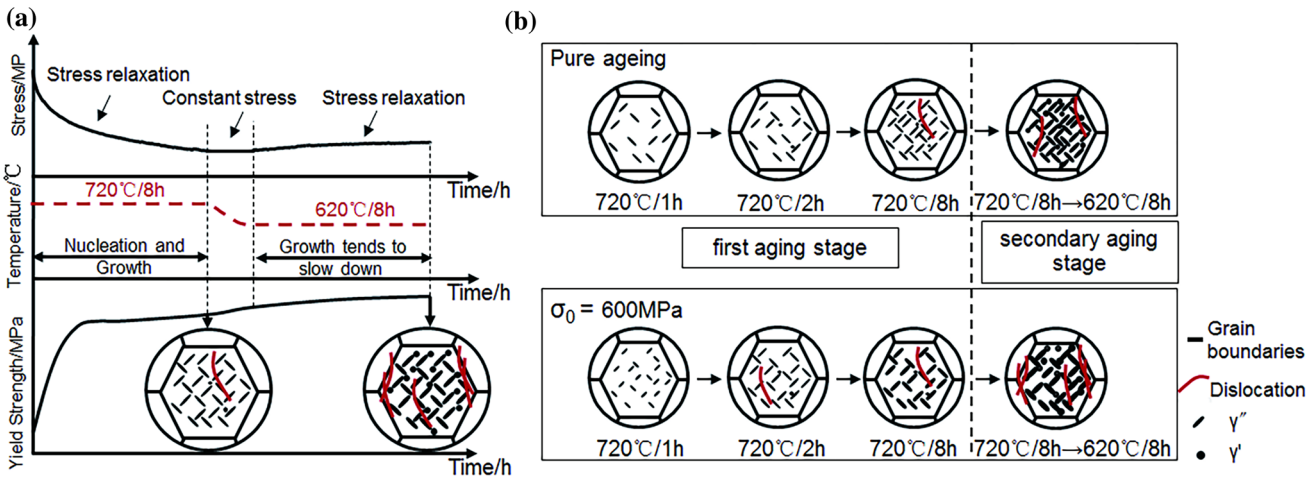

Figure 11 Schematic diagram of **a** the relationship between stress relaxation behavior and age hardening behavior, **b** the evolution of the precipitated phase morphology with different initial loading stresses during the aging process.

When the initial loading stress increases to 600 MPa, more dislocations are activated and begin to move under the combined effect of temperature and loading stress, leading to the increases of sub-structure (see Fig. 6a, d). At this time, the stress relaxation mechanism is dominated as dislocation movement, therefore more elastic deformation has transformed into plastic deformation, which leads to a rapid decrease in stress. In addition, although the amount of sub-structure increased with the application of initial stress, the yield strength of purely aged state presented a relatively higher value due to the significant aging precipitation strengthening effect of the purely aged state. On the other hand, the decrease in the number and density of precipitated phases leads to weakened pinning effect of the dislocations, making the dislocations easier to move and stress relaxation faster.

Conclusions

The stress relaxation behavior and age hardening behavior of Inconel 718 alloy with different initial stress status were investigated after two-stage aging treatment. On basis of the comprehensive analysis on microstructural evolution and mechanical performance, the following conclusions can be obtained:

(1) The stress relaxation behavior of Inconel 718 alloy mainly occurred in the first aging stage. With the initial loading stress increased from 100 to 600 MPa, the corresponding stress relaxation mechanism changed from diffusion creep into dislocation creep, ascribing to the transformation of elastic strain into plastic strain by atomic diffusion or dislocation movement. The stress relaxation behavior of Inconel 718 alloy is closely associated with the initial stress level during the first aging stage.

(2) The stress relaxation occurred in the secondary aging stage was nearly negligible with constant value of stress change, irrespective of initial stress status.

(3) The precipitated behavior of γ'' phase strictly depended on the initial stress status. With increasing initial stress value, dislocation creep was obviously facilitated, leading to relatively faster growth and coarsening of precipitated phase after two-stage aging treatment. As a comparison, the distribution of precipitated phase in sample without initial stress showed relatively more homogeneous and denser, giving rise to a high yield strength.

Acknowledgements

This research did not receive any specific grant from funding agencies in the public, commercial, or not-for-profit sectors.

Declarations

Conflict of interest All authors listed have declared that they have no conflict of interest.

References

[1] Cozar R, Pineau A (1973) Morphology of γ' and γ'' precipitates and thermal stability of Inconel 718 type alloys. Metall Mater Trans B 4:47–59

[2] Miller MK, Babu SS, Burke MG (1999) Intragranular precipitation in alloy 718. Mater Sci Eng A 27:14–18

[3] Azadian S, Wei LY, Warren R (2004) Delta phase precipitation in Inconel 718. Mater Charact 53:7–16

[4] Oblak JM, Paulonis DF, Duvall DS (1974) Coherency strengthening in Ni base alloys hardened by DO_{22} γ′ precipitates. Metall Trans 5:143–153

[5] Sundararaman M, Banerjee S (1992) Some aspects of the precipitation of metastable intermetallic phase in Inconel 718. Metall Trans A 23:2015–2028

[6] Sundararaman M, Mukhopadhya P, Banerjee S (1994) Precipitation and room temperature deformation behavior of Inconel 718. In: Loria EA (ed) Superalloys 718, 625, 706 and various derivatives, The Minerals, Metals and Materials Society, Warrendale, PA, p 419–440

[7] Kirman I, Warrington DH (1970) The precipitation of Ni_3Nb phases in a Ni–Fe–Cr–Nb alloy. Metall Trans 1:2667–2675

[8] Sundararaman M, Mukhopadhyay P, Banerjee S (1988) Precipitation of δ-Ni_3Nb phase in two nickel base Superalloys. Metall Trans A 19:453–465

[9] Sims CT, Hagel WC (1972) The Superallys. Wiley, New York

[10] Sims CT, Stoloff NS, Hagel WC (1987) Superalloys II: high-temperature materials for aerospace and industrial power. Wiley, New York

[11] Rolph J, Evans A, Paradowska A, Hofmann M, Hardy M, Preuss M (2012) Stress relaxation through ageing heat treatment—a comparison between in situ and ex situ neutron diffraction techniques. C R Phys 13:307–315

[12] Aba-Perea PE, Pirling T, Preuss M (2016) In-situ residual stress analysis during annealing treatments using neutron diffraction in combination with a novel furnace design. Mater Des 110:925–931

[13] Rahimi S, King M, Dumont C (2017) Stress relaxation behaviour in IN718 nickel based superalloy during ageing heat treatments. Mater Sci Eng A 708:563–573

[14] Jing Y, He J, Yao ZH, Dong JX (2018) Limitations of calculating stress relaxation limit by function-fitting of Inconel718 superalloy. Mater Lett 221:89–92

[15] Qin HL, Bi ZN, Yu HY, Dong JX (2018) Influence of stress on γ" precipitation behavior in Inconel 718 during aging. J Alloy Compds 740:997–1006

[16] Qin HL, Bi ZN, Li DF, Zhang RY, Lee TL, Feng G, Dong HB, Du JH et al (2018) Study of precipitation-assisted stress relaxation and creep behavior during the ageing of a nickel-iron superalloy. Mater Sci Eng A 742:493–500

[17] Calvo J, Shu SY, Cabrera JM (2012) Characterization of precipitation kinetics of Inconel 718 Superalloy by the stress relaxation technique. Mater Sci Forum 706–709:2393–2399

[18] ASTM International (2013) E328-13 standard test methods for stress relaxation for materials and structures. ASTM International West Conshohohocken. https://doi.org/10.1520/E0328-13

[19] Solberg JK (1986) A semi-empirical model for stress relaxation including primary and secondary creep stages. J Mater Sci 21:630–636. https://doi.org/10.1007/BF01145534

[20] He LZ, Zheng Q, Sun XF, Guan HR, Zhu HT (2005) High temperature creep-deformation behavior of the Ni-based superalloy M963. Metall Mater Trans A 36:2385–2391

[21] Haghighat SMH, Eggeler G, Raabe D (2013) Effect of climb on dislocation mechanisms and creep rates in γ′-strengthened Ni base superalloy single crystals: a discrete dislocation dynamics study. Acta Mater 61:3709–3723

[22] Mukherjee AK, Bird JE, Dorn JE (1968) Experimental correlations for high-temperature creep ASM-Tran 62:155–179

[23] Coble RL (1963) A model for boundary diffusion controlled creep in polycrystalline materials. J Appl Phys 34:1679–1682

[24] Watanable H, Mukai T, Kohzu M, Tanabe S, Higashi K (1999) Effect of temperature and grain size on the dominant diffusion process for superplastic flow in an AZ61 magnesium alloy. Acta Mater 47:3753–3758

[25] Ruano OA, Sherby OD (1988) On constitutive equations for various diffusion-controlled creep mechanisms. Rev Phys Appl 23:625–637

[26] Ruano OA, Wadsworth J, Sherby OD (1985) Deformation mechanisms in an austenitic stainless steel (25Cr-20Ni) at elevated temperature. J Mater Sci 20:3735–3744. https://doi.org/10.1007/BF01113782

[27] Watanabe H, Tsutsui H, Mukai T, Kohzu M, Tanabe S, Higashi K (2001) Deformation mechanism in a coarse-grained Mg–Al–Zn alloy at elevated temperatures. Int J Plast 17:387–397

[28] Somekawa H, Hirai K, Watanabe H, Takigawad Y, Higashi K (2005) Dislocation creep behavior in Mg–Al–Zn alloys. Mater Sci Eng A 407:53–61

[29] Chandler HD (2010) A comparison between steady creep and stress relaxation in copper. Mater Sci Eng A 527:6219–6223

[30] Choudhry MA, Ashraf M (2007) Effect of teat treatment and stress relaxation in 7075 aluminum alloy. J Alloy Compd 437:113–116

[31] Feaugas X, Gaudin C (2001) Different levels of plastic stain incompatibility during cyclic loading: in terms of dislocation density and distribution. Mater Sci Eng A 309–310:382–385

[32] Manjoine MJ (1982) Residual stress and stress relaxation. Springer, New York

[33] Yu XF, Tian SG, Wang MG, Zhang S, Liu XD, Cui SS (2009) Creep behaviors and effect factors of single crystal nickel crystal nickle-base superalloys. Mater Sci Eng A 499:352–359

[34] Zhang JX, Wang JC, Harada H, Koizumi Y (2005) The effect of lattice misfit on the dislocation motion in superalloys during high-temperature low-stress creep. Acta Mater 53:4623–4633

[35] Sun WM, Chen BB, Jin WY, Zeng ZL (1979) Stress relaxation testing. ASTM, West Conshohocken

[36] Ashby MF (1972) A first report on deformation-mechanism maps. Acta Metall 20:887–897

[37] Stouffer DC, Dame LT (1996) Inelastic deformation of metals: models, mechanical properties, and metallurgy. Wiley, New York

[38] Sinha NK, Sinha S (2005) Stress relaxation at high temperatures and the role of delayed elasticity. Mater Sci Eng A 393:179–190

[39] Sinha NK (2003) Limitations of stress relaxation tests for determining stress dependence of strain rate at high temperature. Scr Mater 48:731–736

[40] Srinivasan R, Eggeler GF, Mills MJ (2000) γ′—cutting as rate-controlling recovery process during high temperature and low-stress creep of superalloy single crystals. Acta Mater 48:4867–4878

[41] Fisk M, Ion JC, Lindgren LE (2014) Flow stress model for IN718 accounting for evolution of strengthening precipitates during thermal treatment. Comput Mater Sci 82:531–539